

Dynamical Effects in Confined Plasma Turbulence

**I. L. Caldas, R. L. Viana,
Z. O. Guimarães-Filho, A. M. Batista,
S. R. Lopes, F. A. Marcus, M. Roberto,
K. C. Rosalem, J. D. Szezech, et al**

Brazilian Journal of Physics

ISSN 0103-9733

Braz J Phys

DOI 10.1007/s13538-014-0259-x



Your article is protected by copyright and all rights are held exclusively by Sociedade Brasileira de Física. This e-offprint is for personal use only and shall not be self-archived in electronic repositories. If you wish to self-archive your article, please use the accepted manuscript version for posting on your own website. You may further deposit the accepted manuscript version in any repository, provided it is only made publicly available 12 months after official publication or later and provided acknowledgement is given to the original source of publication and a link is inserted to the published article on Springer's website. The link must be accompanied by the following text: "The final publication is available at link.springer.com".

Dynamical Effects in Confined Plasma Turbulence

I. L. Caldas · R. L. Viana · Z. O. Guimarães-Filho · A. M. Batista ·
S. R. Lopes · F. A. Marcus · M. Roberto · K. C. Rosalem ·
J. D. Szezech Jr. · D. Toufen · K. W. Gentle ·
I. C. Nascimento · Y. K. Kuznetsov

Received: 30 April 2014
© Sociedade Brasileira de Física 2014

Abstract Plasma turbulence at the edge of tokamaks is an issue of major importance in the study of the anomalous transport of particles and energy. Although the behavior of a turbulent plasma seems intractable, it turns out that many of its aspects can be described by low-dimensional non-integrable dynamical models. In this paper, we consider a number of dynamical effects occurring in tokamak plasma edge—in particular the role of internal transport barriers. Furthermore, we present experimental results on turbulent-driven transport for two machines—the Brazilian TCABR tokamak and University of Texas' Helimak—that can be explained by those theoretical models.

Keywords Plasma turbulence · Non-twist systems · Wave mode coupling · Tokamaks

1 Introduction

One of the key theoretical problems in the physics of magnetically confined fusion plasmas is the causes and associated rates of anomalous cross-field transport [1, 2]. There exists a widespread consensus that turbulence plays a major role on the mechanisms leading to anomalous transport [3–5]. Turbulent processes display a broad fluctuation spectra with maxima corresponding to small wave vectors and high frequencies [6, 7]. A candidate for explaining the observed anomalous transport rates in tokamaks is drift wave turbulence, thanks to the presence of steep density gradients in the plasma edge [8].

One of the characteristic features of a turbulent plasma is the presence of a very large number of degrees of freedom. However, we assume that, at least in some types of turbulence, it is possible to capture the essential features of turbulent system using low-dimensional dynamical systems. This approach was introduced in the seminal paper from Ruelle and Takens [10] and has led to a deeper understanding of the dynamical mechanisms underlying the onset of turbulence. If the system is sufficiently dissipative, its dynamics is governed by a low-dimensional chaotic attractor embedded in a phase space with a large number of dimensions. The dynamics in this attractor can thus be described by simpler systems; the Lorenz equations being one of the well-known examples of how this dimensional reduction procedure can provide useful information about the turbulence of a fluid system [11].

In this paper, we report basic ideas that we have applied to identify low-dimensional dynamical effects in turbulence,

Dedicated to Professor Wendell Horton for his outstanding contributions to the nonlinear dynamics approach to plasma turbulence.

I. L. Caldas · Z. O. Guimarães-Filho · F. A. Marcus ·
I. C. Nascimento · Y. K. Kuznetsov
University of São Paulo, São Paulo, São Paulo, Brazil

R. L. Viana (✉) · S. R. Lopes
Federal University of Paraná, Curitiba, Paraná, Brazil
e-mail: viana@fisica.ufpr.br

A. M. Batista · J. D. Szezech Jr.
State University of Ponta Grossa, Ponta Grossa, Paraná, Brazil

M. Roberto · K. C. Rosalem
Aeronautical Technological Institute, São José dos Campos,
São Paulo, Brazil

D. Toufen
Federal Institute of São Paulo, Guarulhos, São Paulo, Brazil

K. W. Gentle
The University of Texas at Austin, Austin, USA

particularly related to drift waves and particle transport at plasma edge [8, 9]. Furthermore, we describe how these dynamical effects have been applied for the plasma turbulence observed in TCABR Tokamak (University of São Paulo, Brazil) and Texas Helimak (University of Texas at Austin) to understand the reduction of turbulence-induced transport by the formation of internal transport barriers. All these described evidences of non-linear effects in plasma physics have been obtained by applying models and procedures introduced by Horton [2]. We have already described these evidences separately in previous publications; however, the present article puts them in a common perspective and illustrates some Hortons contributions to the plasma turbulence theory.

The rest of the paper is organized as follows: In Section 2, we consider a simplified model for drift-wave turbulence involving non-linear wave coupling in which we emphasize both the onset of turbulence as well as the energy transfer processes. We also consider the control of chaotic behavior through the addition of a fourth resonant wave. Section 3 considers the formation of internal transport barriers and their dependence on non-monotonic profiles, as in reversed shear plasma flows. We first consider a simplified dynamical model, the standard non-twist map, which exhibits the formation of a shearless curve which acts as an internal transport barrier.

A physical model for the $\mathbf{E} \times \mathbf{B}$ drift motion of particles in a magnetized plasma also presents the formation of such a barrier due to a non-monotonic electric field radial profile. We then consider experimental evidences of the internal transport barrier formation in the TCABR tokamak and Helimak. Finally, we consider a theoretical model for the influence of magnetic shear on the internal transport barriers. The last section is devoted to our conclusions.

2 Non-linear Wave Coupling

2.1 Prediction of Three-Wave Coupling

Hasegawa and Mima obtained in 1977 a non-linear partial differential equation which describes the propagation of drift waves in magnetized plasmas and the emergence of stationary, non-uniform turbulence [12]:

$$\frac{\partial}{\partial t} (\nabla^2 \phi - \phi) - [(\nabla \phi \times \hat{\mathbf{z}}) \cdot \nabla] \left[\nabla^2 \phi - \ln \left(\frac{n_0}{\omega_{ci}} \right) \right] = 0, \tag{1}$$

where $\phi(\mathbf{x}, t)$ is the electrostatic potential of a wave with frequency ω propagating through an inhomogeneous plasma where there is a uniform magnetic field $\mathbf{B} = B_0 \hat{\mathbf{e}}_z$. The wave frequency must be less than the ion cyclotron frequency

$\omega_{ci} = eB_0/m_i$, where e and m_i are, respectively, the charge and mass of the ions, and n_0 is the background plasma density. The operator ∇ in Eq. (1) denotes the gradient in the directions transverse to the magnetic field.

Although neglecting effects expected in plasma edge tokamaks, as those due to the toroidal curvature or the dynamics along the field line, the Hasegawa-Mima equation is still considered a good model to investigate the relevance of the non-linear mode coupling considered in our work.

A linear wave exists in this situation if the phase velocity along the magnetic field is such that $v_{Ti} < (\omega/k_z) < v_{Te}$, where v_{Ts} is the thermal velocity for ions ($s = i$) and electrons ($s = e$). For long wavelengths, this is a drift wave in which the dispersion relation is $\omega = \mathbf{k} \cdot \mathbf{v}_d$, where \mathbf{v}_d is the diamagnetic drift velocity. Moreover, drift waves possess a characteristic dispersion scale length $\rho_s = \sqrt{T_e/m_i}/\omega_{ci}$ [9].

We seek solutions for the Hasegawa-Mima (1) by Fourier-expanding the electrostatic potential

$$\phi(x, t) = \frac{1}{2} \sum_{k=1}^{\infty} [\phi_{\mathbf{k}}(t) \exp(i\mathbf{k} \cdot \mathbf{x}) + c.c.], \tag{2}$$

where the $\phi_{\mathbf{k}}(t)$ are the electrostatic modes in Fourier space. The substitution of (2) into (1) yields an infinite system of coupled differential equations for the Fourier modes [9, 13]. In fact, however, it suffices to analyze a few modes when the turbulence is not yet fully developed [14, 15].

Accordingly, we consider a three-wave truncation of (2), whose wave vectors satisfy the triplet condition $\mathbf{k}_1 + \mathbf{k}_2 + \mathbf{k}_3 = \mathbf{0}$. Moreover, we introduce phenomenological dissipative terms γ_i that describe mode growth or decay, yielding the system

$$\frac{d\phi_1}{dt} + i\omega_1\phi_1 = \Lambda_{2,3}^1 \phi_2^* \phi_3^* + \gamma_1 \phi_1, \tag{3}$$

$$\frac{d\phi_2}{dt} + i\omega_2\phi_2 = \Lambda_{3,1}^2 \phi_3^* \phi_1^* + \gamma_2 \phi_2, \tag{4}$$

$$\frac{d\phi_3}{dt} + i\omega_3\phi_3 = \Lambda_{1,2}^3 \phi_1^* \phi_2^* + \gamma_3 \phi_3, \tag{5}$$

where we denoted $\phi_j(t) = \phi_{\mathbf{k}_j}(t)$ and $\omega_j = \omega_{\mathbf{k}_j}$ and the coupling coefficients are given by [16]

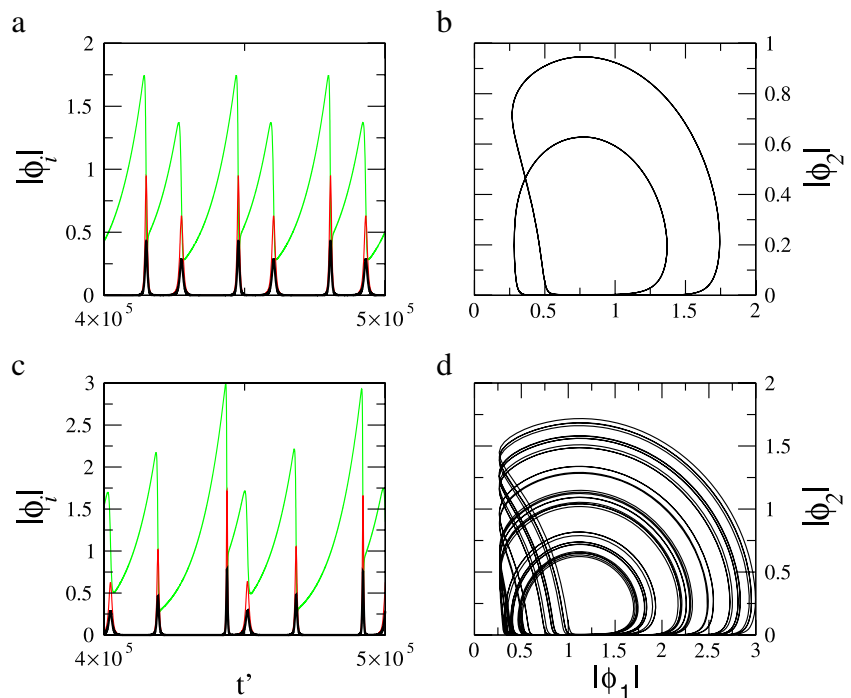
$$\Lambda_{2,3}^1 = \frac{(k_3^2 - k_2^2)}{2(1 + k_1^2)} (\mathbf{k}_2 \times \mathbf{k}_3) \cdot \hat{\mathbf{z}} \tag{6}$$

$$\Lambda_{3,1}^2 = \frac{(k_1^2 - k_3^2)}{2(1 + k_2^2)} (\mathbf{k}_3 \times \mathbf{k}_1) \cdot \hat{\mathbf{z}} \tag{7}$$

$$\Lambda_{1,2}^3 = \frac{(k_2^2 - k_1^2)}{2(1 + k_3^2)} (\mathbf{k}_1 \times \mathbf{k}_2) \cdot \hat{\mathbf{z}} \tag{8}$$

In the following, we adopt parameters from the TCABR tokamak of University of São Paulo: major radius $R = 61$ cm, minor radius $a = 18$ cm, maximum plasma

Fig. 1 Time series of the wave amplitudes $|\phi_i|$ [$i = 1$ (green), $i = 2$ (red), and $i = 3$ (black)] for γ_2 equal to **a** -0.002 and **c** -0.003 . **b** and **d** are the phase space projections corresponding to **a** and **c**, respectively

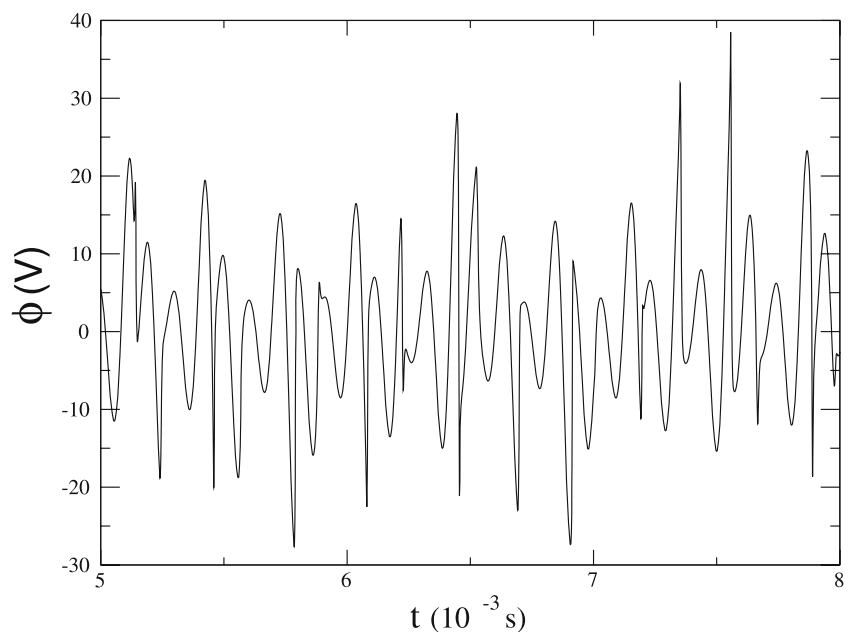


current 100 kA, plasma duration 100 ms, hydrogen filling pressure 3×10^4 Pa, and toroidal magnetic field $B_0 = 1.1$ T. At the plasma edge, the electron plasma density is $n_e = 3 \times 10^{18} \text{ m}^{-3}$ and the electron temperature is $T_e = 10$ eV. The ratio between the density gradient and the density in this region has been estimated as 1 cm^{-1} . Fluctuations of the floating potential at plasma edge have a poloidal wave number k_θ in the range of $1 - 5 \times 10^3 \text{ m}^{-1}$, with broad spectral content pronounced in the $1 - 100 \text{ kHz}$ range. We thus have chosen the mode frequencies as $\omega_1 =$

$\omega_2 = \omega_3 = 50 \text{ kHz}$. As for the wave numbers, we choose $k_{x1} = 4.5 \text{ cm}^{-1}$, $k_{y1} = 6.5 \text{ cm}^{-1}$ and the others are expressed in terms of them as follows: $k_{x2} = 0.1k_{x1}$, $k_{x3} = -1.1k_{x1}$, $k_{y2} = 2.0k_{y1}$, and $k_{y3} = -3.0k_{y1}$.

The numerical values of the growth/decay rates have been adjusted to get wave amplitudes in the range observed in experiments of plasma edge fluctuations, namely $-50\text{V} - +50\text{V}$, namely $\gamma_1 = 0.0001$, $\gamma_2 = \gamma_3 \in [-0.0015, -0.003]$, the latter being our control parameter. With this set of parameters, the three-wave equations are

Fig. 2 Time series of the potential in the real domain for the same parameters as those of Fig. 1c, d



numerically integrated. Figure 1a displays the time series of the wave amplitudes $|\phi_i|$ for $\gamma_2 = -0.002$, showing a period-2 orbit in the corresponding phase space projection (Fig. 1b). This attractor becomes chaotic at $\gamma_2 = -0.003$ (Fig. 1c, d).

On fixing the point $x = y = 0$, we obtain the time series corresponding to the “real” electrostatic signal given by the sum of the three Fourier modes for the chaotic case, resulting in Fig. 2. The dependence of the wave dynamics on the control parameter γ_2 is illustrated by the bifurcation diagram shown in Fig. 3a, where we depict the asymptotic values of the discrete variable $z_n := \max |\phi_1|$. The corresponding maximum Lyapunov exponent is represented in Fig. 3b. Chaotic behavior occurs for $\gamma_2 \lesssim -0.0023$ interspersed with windows of periodic behavior.

2.2 Resonant Control of Oscillations

One of the key points of the present analysis is that chaotic behavior in the drift-wave dynamics is directly related to the appearance of turbulent fluxes and anomalous transport in the tokamak plasma edge. Hence, once we have a low-dimensional model of this situation, as explained in the previous subsection, a relevant question is how to control these chaotic oscillations so as to reduce or utterly eliminate turbulence in this region.

One possible control strategy is the addition of a resonant fourth mode with small amplitude. In this case, a resonant four-wave coupling involves the interaction of two-wave

triplets. The presence of the second triplet having two waves in common with the first can increase or stabilize the instability of the first triplet [17, 18]. Accordingly, we introduce a fourth wave ϕ_4 , which adds a second wave triplet obeying the resonant conditions: $\mathbf{k}_4 = \mathbf{k}_1 + \mathbf{k}_2$ and $\omega_4 \approx \omega_1 + \omega_2$. The amplitude of the control wave is kept small so that $|\phi_4| \equiv \epsilon \ll |\phi_{1,2,3}|$ and constant so that $d\epsilon/dt = 0$. Inserting the control wave in the three-wave system amounts to add a term $|\epsilon|\phi_2^*$ to (3) and a term $|\epsilon|\phi_1^*$ to (4) [19].

The addition of a fourth resonant wave, with an amplitude as small as $\epsilon = 10^{-10}$, is already enough to steer the phase-space trajectory to a period-8 orbit. Other orbits with periods equal to 4 and 2 can be obtained using different values of ϵ . The dependence of the dynamics on ϵ is illustrated by the bifurcation diagram depicted in Fig. 4 in which we plot the asymptotic values of $\max |\phi_2|$ versus the strength of the resonant perturbation ϵ , the remaining parameters being held constant. On increasing the values of ϵ , we have a less complex dynamics, starting from a one-band chaotic attractor followed by various windows of periodic behavior, two-band chaotic attractors, towards low-period orbits.

3 Particle Transport Barriers

Internal transport barriers have been observed in many systems of interest for plasma physics. One of them is radial particle transport in toroidal plasma devices with reversed magnetic shear [20] and the $\mathbf{E} \times \mathbf{B}$ -drift motion of charged particles in a magnetized plasma under the action of a time-periodic electric field from an electrostatic wave [21, 22]. In both cases, the internal transport barriers cause an overall reduction of radial particle and energy transfer, which has direct consequences on the duration and quality of plasma confinement.

Here, we describe internal transport barriers created by applying a perturbing electric field in the tokamak edge region comprising the plasma edge and the scrape-off layer, where the plasma exhibits high level of electrostatic turbulence-induced particle transport [36]. Besides that, we also show how such transport barriers can be created in the perturbed helimak discharges.

3.1 Shearless Transport Barriers in Non-twist Maps

In order to study the mechanisms whereby particle transport barriers occur in tokamak plasmas, we first consider simple models for magnetic field line behavior. It turns out that these internal barriers exist in plasmas with non-monotonic equilibrium zonal flows, giving rise to orbit topologies that can only exist with reversed shear [21], i.e., with a non-monotonic rotation number profile. The barriers appear in the shearless region of non-twist Hamiltonian systems and display their own typical characteristics with a proper route

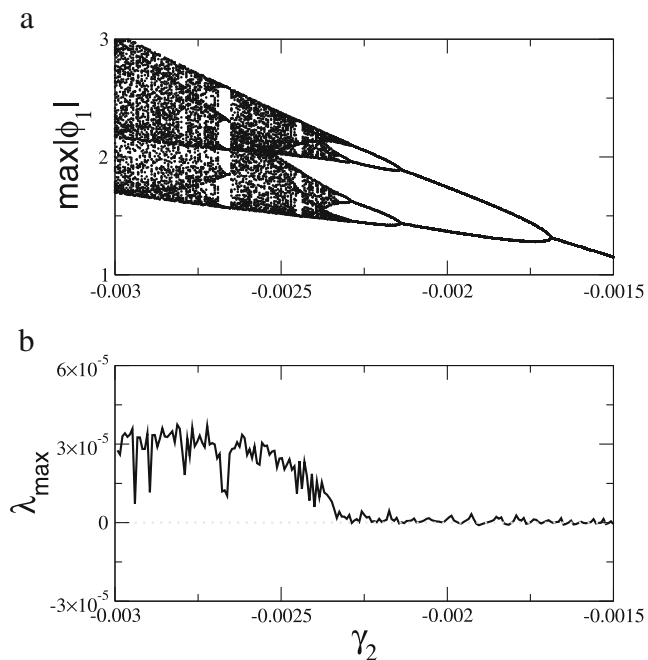
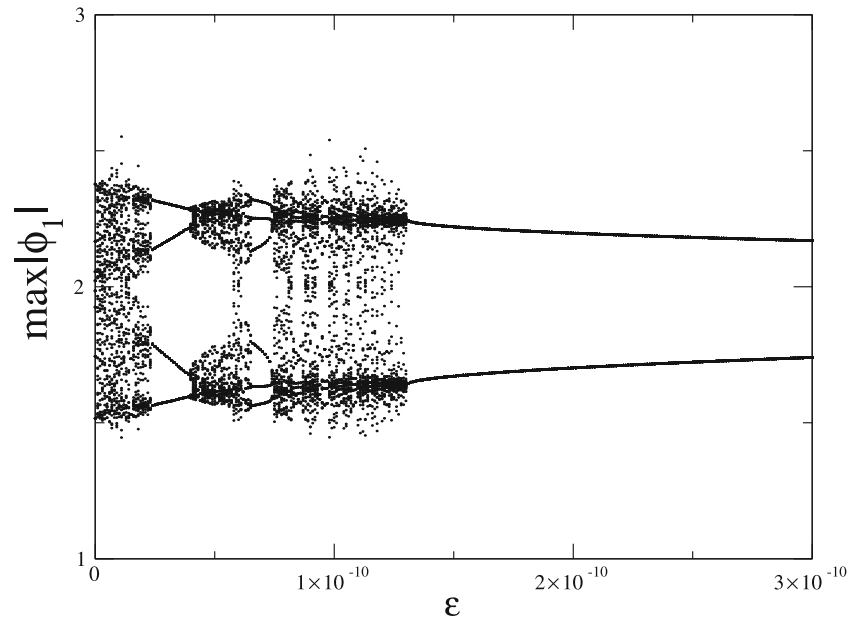


Fig. 3 **a** Bifurcation diagram for the discrete variable $\max |\phi_1|$ for $\gamma_1 = 0.0001$ and varying γ_2 . **b** Maximum Lyapunov exponent

Fig. 4 Bifurcation diagram for the asymptotic values of $\max|\phi_2|$ vs the amplitude of the controlling wave for $\gamma_1 = 0.0001$ and $\gamma_2 = -0.0025$



of transition to chaos [23]. These barriers are robust in the sense that they persist even for high amplitude perturbations and have an effective capacity to reduce the transport even after invariant tori are broken [24]. The mechanism underlying the capacity to reduce transport is the stickiness around magnetic islands that remain in the shearless region after the tori disappear [25].

A simple system which exhibits this phenomenology is the standard non-twist map [23]

$$x_{n+1} = x_n + a(1 - y_{n+1}^2), \tag{9}$$

$$y_{n+1} = y_n - b \sin(2\pi x_n), \tag{10}$$

where $x \in [-1/2, +1/2]$, $y \in \mathbb{R}$, $a \in (0, 1)$, and $b > 0$. In terms of a tokamak, the discrete variables (x_n, y_n) can be thought of the coordinates of the n th piercing of an equilibrium magnetic field line with a toroidal surface of section.

The winding number of this symplectic map, namely $g(y) = -a(1 - y_{n+1}^2)$, corresponds to the safety factor of the corresponding magnetic surfaces and it is non-monotonic since its derivative (magnetic shear) changes sign, violating the so-called twist condition. This is why the map Eqs. (9)–(10) is called non-twist. The loci where $g'(y_S) = 0$, i.e., where the shear changes sign, define shearless curves in phase space: $\{(x, y) | -1/2 \leq x < 1/2, y = y_S = 0\}$. Hence, the parameter a stands for the non-twist character of the map.

The parameter b in Eq. (10) plays the role of the perturbation strength. When it is non-zero, two periodic island chains appear at the two invariant curve locations, and the former shearless curve becomes a shearless invariant torus separating these two island chains with three islands each,

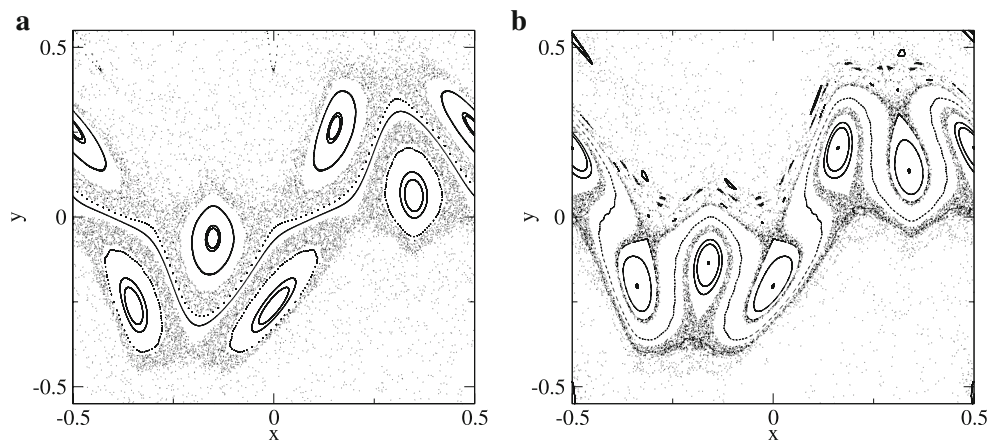
with winding number 1/3 (Fig. 5a). The local maxima of the perturbed winding number profile define a shearless invariant curve, whose existence can be inferred between the two island chains. There are also chaotic layers in the neighborhoods of both island chains, although these layers are not connected, thanks to the existence of invariant curves near the shearless invariant tori [26].

If the parameters a and b are slightly modified, the two island chains with the same winding number approach each other and their unstable and stable invariant manifolds suffer reconnection (Fig. 5b). In the region between the chains, there appears new invariant tori called meandering curves. The periodic orbits remaining coalesce, as the parameters are further modified, and eventually leave only meanders and the shearless torus (Fig. 6a). The set of meanders and the shearless torus is an internal transport barrier for the chaotic orbits on the different sides of the barrier are kept segregated. Further alterations of the parameters cause the breakup of the shearless torus and meanders, destroying the internal transport barriers and allowing the mixing of the formerly segregated chaotic orbits (Fig. 6b).

3.2 Internal Transport Barriers in Plasmas

The scenario for the creation of internal transport barriers we described in the previous subsection is simple enough to allow for a detailed treatment, but in order to apply it to the tokamak context, we need a more detailed physical model. We already pointed out that the internal transport barriers occur in the plasma edge region of tokamaks, where turbulence prevails. Such turbulence is associated with drift waves that propagate in the poloidal direction and are driven

Fig. 5 Phase portraits of the standard non-twist map Eqs. (9)–(10) for $b = 0.4$ and **a** $a = 0.70$; **b** $a = 0.69$



by radial density gradients [9]. As a matter of fact, experiments suggest that particle transport in the tokamak plasma edge is chiefly caused by $\mathbf{E} \times \mathbf{B}$ particle drifts [8].

Hence, a simple but physically sound model consists on the particle dynamics in a toroidal equilibrium magnetic field $\mathbf{B} = B_0 \hat{e}_z$ subjected to electrostatic drift waves propagating along the poloidal direction \hat{e}_y . The radial direction points to \hat{e}_x . The drift velocity of the guiding centers is $\mathbf{v} = \mathbf{E} \times \mathbf{B}/B^2$, where $\mathbf{E} = -\nabla\phi(x, y, t)$ and [27]

$$\overline{\phi(x, y, t)} = \phi_0(x) + \sum_{i=1}^N A_i \sin(k_{x_i}x) \cos(k_{y_i}y - \omega_i t), \quad (11)$$

representing a background static potential plus the superposition of N drift waves with amplitudes A_i , wave numbers k_i , and frequencies ω_i . Assuming that particles are passively advected by the $\mathbf{E} \times \mathbf{B}$ drift velocity, we can write their equations of motion in a canonical form

$$\frac{dx}{dt} = -\frac{\partial H}{\partial y}, \quad \frac{dy}{dt} = \frac{\partial H}{\partial x}, \quad (12)$$

where $H(x, y, t) = \phi/B_0$ is the Hamiltonian function. The case of only one drift wave ($N = 1$) turns out to be inte-

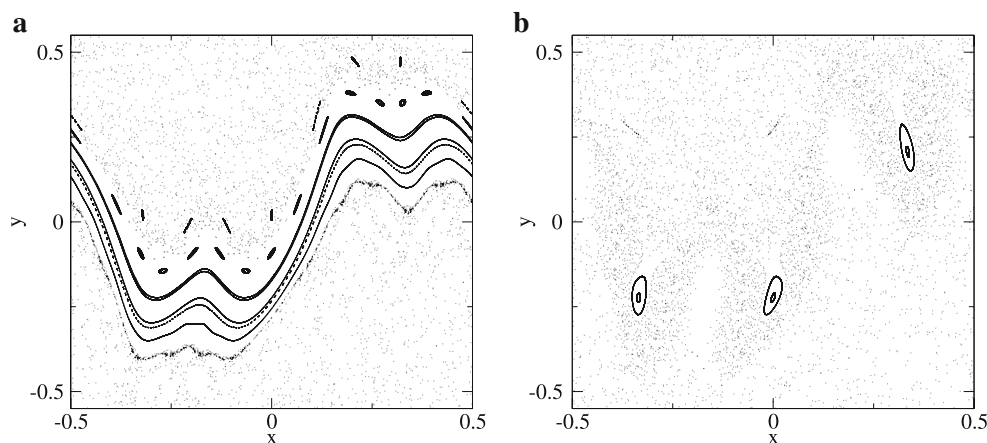
grable, with Hamiltonian (in a reference frame moving with the phase velocity of the wave $u_1 = \omega_1/k_{y_1}$):

$$H(x, y) = \frac{\phi_0(x)}{B_0} - u_1 x + \frac{A_1}{B_0} \sin(k_{x_1}x) \cos(k_{y_1}y). \quad (13)$$

The static contribution for the poloidal flow drift velocity is $v_E(x) = (1/B_0)(d\phi_0/dx)$, such that $\dot{y} \sim v_E - u_1 = U$, where U is called trapping parameter. It vanishes when there is a resonance between the phase velocity of the wave and the static drift velocity. The dynamical (12) were integrated numerically. There results a tiling of the phase space in islands representing particles trapped in the wave field (Fig. 7a).

If the trapping parameter is non-zero but uniform, there exist both periodic islands and invariant curves in the phase space (Fig. 7b). Now, we consider the existence of a non-monotonic electric field radial profile, as the field produced by a bias electrode inserted radially into the plasma column. As we shall see in the following subsections, this procedure has been able to reduce particle transport in the tokamak plasma edge. We will show that, already in this simple model, this reduction comes from the formation of

Fig. 6 Phase portraits of the standard non-twist map Eqs. (9)–(10) for $b = 0.5$ and **a** $a = 0.68$; **b** $a = 0.70$



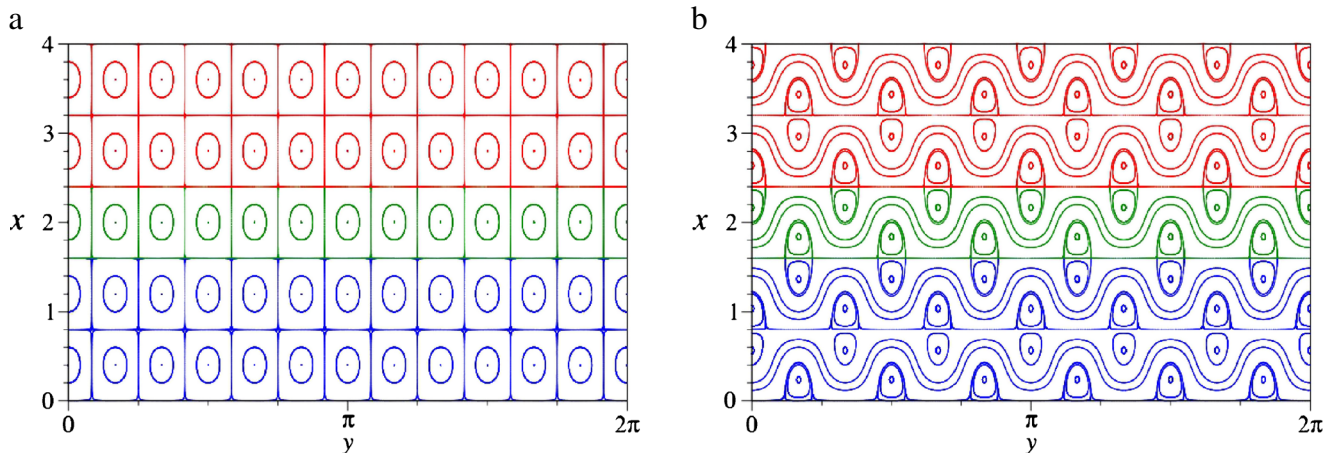


Fig. 7 Phase portrait of the dynamical system obtained from the integrable one-wave Hamiltonian (13) with **a** $U = 0$ and **b** $U = 0.6$

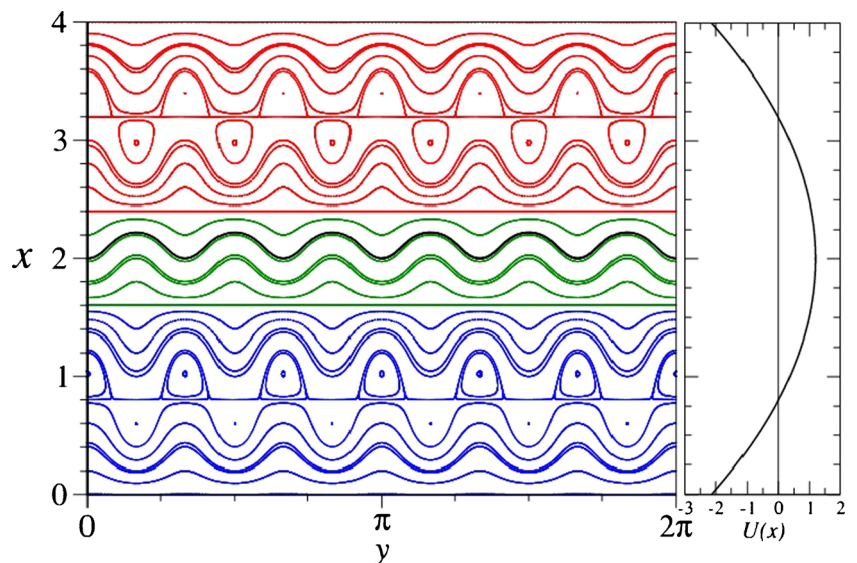
an internal transport barrier. The radial profile we choose for the trapping parameter is [28]

$$U(x) = \frac{1}{Ak_x} [a_2x^2 + a_1x + (a_0 - u)], \tag{14}$$

where $a_2 = -0.84$, $a_1 = 3.34$, $a_0 - u = -2.1334$, $A = 0.16$, and $k_x = 3.9267$.

In this case, the trapping parameter is no longer uniform but rather presents a non-monotonic radial profile (see the right panel in Fig. 8): it has a global maximum inside the plasma column, where a shearless curve is produced. Just like in the standard non-twist map, the shearless curve is an internal transport barrier. Since the one-wave Hamiltonian represents an integrable system, there are no chaotic (area-filling) orbits in this case. However, if we consider the presence of two or more drift waves, there will appear chaotic regions on both sides of the shearless curve.

Fig. 8 Phase portrait of the dynamical system obtained from the integrable one-wave Hamiltonian (13) with a non-monotonic radial profile for the trapping parameter



3.3 Transport Barriers in TCABR Tokamak

Transport barriers were experimentally observed in plasma discharges of the TCABR machine (Tokamak Chauffage Alfvén Brésilien), which operates in the Institute of Physics of the University of São Paulo [29]. In this subsection, we will show recent results showing the reduction of radial particle transport driven by turbulent flux in the plasma edge region. A non-monotonic electric field profile is created by introducing a biased electrode in the tokamak [30]. We interpret the experimental results by the creation of internal transport barriers due to the non-monotonic radial electric field, according to the theoretical framework described in the previous subsection.

Figure 9 shows the time evolution of the spectral contribution of the radial transport driven by turbulent flux in the scrape-off layer of TCABR tokamak. In Fig. 9a, b, we consider the application of an external bias potential of +100 V

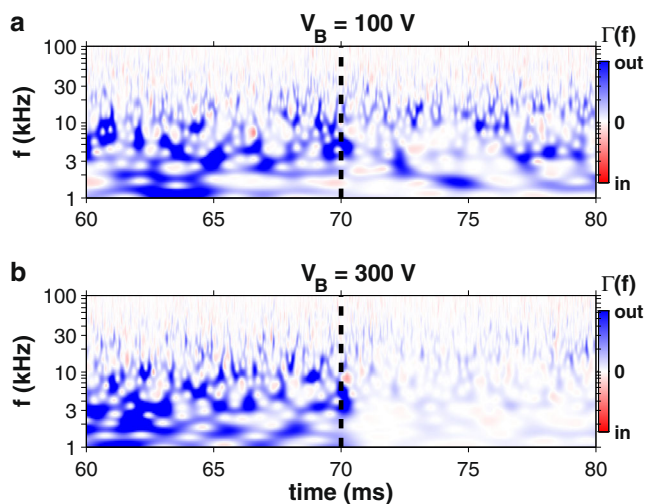


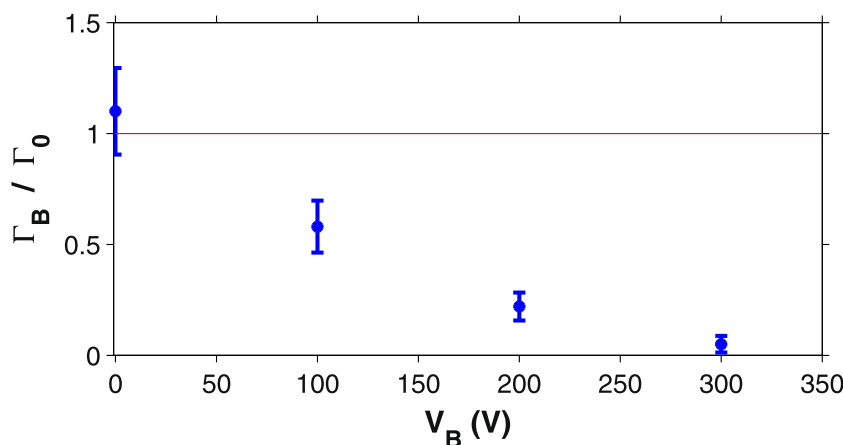
Fig. 9 Spectral contribution of the radial transport driven by turbulent flux (in color scale) in the SOL of TCABR for bias voltages of **a** 100 V and **b** 300 V

and +300 V, respectively, at the time instant indicated by a dashed line in the middle of both figures. Before the application of the bias potential, the radial transport is concentrated at low frequencies (in the frequency range of 1 – 10 kHz). We also see that the spectral contribution of turbulent transport is considerably reduced after the application of low bias (Fig. 9a) and practically disappears for high bias (Fig. 9b) [31–33].

The reduction of turbulent transport due to bias can be also appreciated by computing the time-averaged turbulent flux before (Γ_0) and after (Γ_B) the application of an external bias. Figure 10 shows the ratio Γ_B / Γ_0 as a function of the bias potential. If no bias is applied at all, this ratio is (within the considered uncertainty) equal to the unity, as expected. As the bias voltage is increased up to +300 V, the turbulent flux decreases and practically disappears.

This scenario is explained by the formation of a transport barrier due to a non-monotonic radial electric field profile,

Fig. 10 Ratio between the time-averaged turbulent fluxes with and without external bias as a function of the bias voltage for TCABR discharges



as explained in the previous subsection. If no bias is applied, this transport barrier is located outside the plasma column (in the scrape-off layer) and hardly affects particle transport in the plasma. As a bias voltage is applied, though, this transport barrier migrates into the plasma and reduces dramatically turbulent fluxes in this region, as suggested by experimental data [31–33].

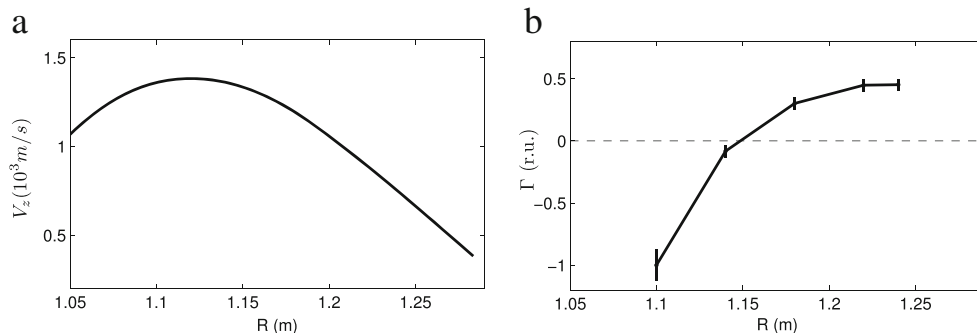
3.4 Transport Barriers in Texas Helimak

Another machine in which we have investigated experimentally the formation of internal transport barriers is the Texas Helimak, which is a toroidal device with a plasma colder and less dense than a tokamak plasma, in such a way that a Helimak reproduces the conditions prevailing in the scrape-off layer of a tokamak [34, 35]. In particular, the Helimak is suitable for experimental studies of plasma edge turbulence and transport of interest in advanced tokamak scenarios.

In the Texas Helimak, there is a basic toroidal magnetic field (0.1 T) and a small vertical field, whose combination leads to helical magnetic field lines, most of them starting and terminating into sets of collector plates located at the top and bottom parts of the vessel. Its dimensions are 1.6 m (external radius), 0.6 m (internal radius), and 2.0 m (height). Thanks to the low density of the plasma, there are many Langmuir probes mounted at the collector plates, enabling us to measure radial profiles of the ion saturation current and mean floating potential [36].

The collector plates can also be used to introduce a bias electric field, just as we have considered before for the TCABR machine. Combined with the toroidal magnetic field, there is a $\mathbf{E} \times \mathbf{B}$ drift along the vertical direction, whose (non-monotonic) radial profile is depicted in Fig. 11a, presenting a maximum at 1.13 m wherein a shearless barrier appears, such that there is a sheared flow around this position.

Fig. 11 **a** Radial profile of the vertical plasma velocity measured through a Doppler shift spectrometer for bias +10 V. **b** Radial profile of the turbulence induced radial particle transport for bias +10 V



We considered the density and drift velocity fluctuations to calculate the particle transport induced by the electrostatic turbulence. Within this procedure, the time-averaged transport flux is given by $\Gamma = \langle \tilde{n} \cdot \tilde{V}_E \rangle$, where \tilde{n} and \tilde{V}_E are, respectively, the density and the $\mathbf{E} \times \mathbf{B}$ electric drift velocity fluctuations [37]. In Fig. 11b, we show a radial profile of the transport flux, showing that at the vicinity of the shearless barrier, the transport flux is nearly 0, i.e., a strong reduction of transport due to the internal barrier.

3.5 Influence of Magnetic Shear on the Transport Barriers

In this subsection, we will consider the drift-kinetic model to investigate the role of the electric and magnetic shears in the particle transport driven by drift wave electrostatic fluctuations in the plasma edge. In this case, the guiding center motion $\mathbf{x}(t)$ is described by the equation [22]

$$\frac{d\mathbf{x}}{dt} = v_{\parallel} \frac{\mathbf{B}}{B} + \frac{\mathbf{E} \times \mathbf{B}}{B^2}, \quad (15)$$

where we have used local (pseudo-toroidal) coordinates $\mathbf{r} : (r, \theta, \varphi)$, v_{\parallel} is the guiding center velocity parallel to \mathbf{B} , which is the equilibrium magnetic field, and $\mathbf{E} = -\nabla\phi$, where $\phi = \phi_0 + \tilde{\phi}$, with a background electric potential ϕ_0 (with a given radial profile) and the fluctuating potential is given by

$$\tilde{\phi}(\mathbf{x}, t) = \sum_{m,\ell,n} \phi_{m\ell n} \cos(m\theta - \ell\varphi - n\omega_0 t - \psi_0), \quad (16)$$

where $\phi_{m\ell n}$ are the mode amplitudes, ω_0 is the lowest angular frequency with substantial amplitude in the drift wave spectrum, and ψ_0 is a random phase. For a single spatial M/L mode, we have considered a drift wave spectrum given by a maximum amplitude, namely ϕ_{MLn} , at the plasma edge resonance and a minimum amplitude inside the plasma core.

For convenience, we also consider action and angle variables for the equations of guiding center motion as $I = (r/a)^2$ and $\psi = M\theta - L\varphi$ respectively, where a is the plasma radius and (M, L) are the poloidal and toroidal mode numbers of the dominant modes. Note here that ψ

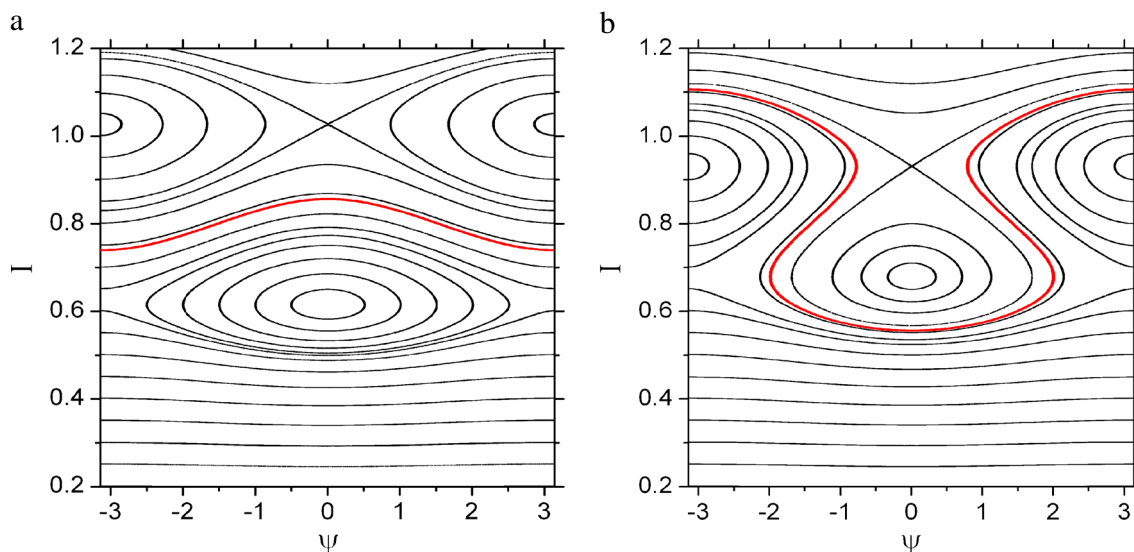


Fig. 12 Phase portraits for the system described by Eqs. (17)–(18) for a non-monotonic background electric field profile and safety factor profiles with **a** $q(a) = 6$ and **b** $q(a) = 4$ at the plasma edge. The shearless curves are depicted in red

plays the role of a helical angle for these modes (coherent oscillations). Taking these assumptions into (15), it is written in a canonical form:

$$\frac{dI}{dt} = \frac{2M}{Ba^2} \sum_{M,L,n}^N \phi_{MLn} \sin(\psi - n\omega_0 t - \psi_0), \quad (17)$$

$$\frac{d\psi}{dt} = \frac{v_{\parallel}}{Rq(I)} [M - q(I)L] - \frac{ME_r}{Ba\sqrt{I}}, \quad (18)$$

where R is the Tokamak major radius and $q(I)$ is the safety factor profile in local coordinates. We also used a non-monotonic radial profile for the background electric field due to drift waves $E_r = -\partial\phi_0/\partial r$.

The above set of equation were numerically integrated for a dominant mode with $M/L = 4/16$, $n = 3$, and an amplitude $\phi_{4,16,n} = 4eV$ for an equilibrium with safety factor at the plasma edge $q(a)$ equal to 6 (Fig. 12a) and 4 (Fig. 12b). The non-monotonic profile we adopted for $E(r)$ is such that there are two twin islands for $n = 3$ separated by a shearless curve. As the value of $q(a)$ is decreased, though, there are reconnection processes and there results an internal transport barriers. Hence, the latter is modified by the magnetic shear and persist under variations of $q(a)$.

4 Conclusions

The unifying element in this paper is the possibility of describing plasma edge turbulence in terms of low-dimensional dynamical systems that enables us to explain (at least qualitatively) results of experiments on transport performed in two machines: the Brazilian TCABR tokamak and the Texas Helimak. We have also obtained, with the help of these low-dimensional models, a number of theoretical results concerning the onset and evolution of wave turbulence at the plasma edge of both TCABR and Helimak. This low-dimensional description is based in a drift wave three-mode coupling, such that turbulent behavior stems from a modulational instability. The transition between laminar and chaotic behavior can be controlled by an external resonant wave.

The observed turbulent-driven transport in plasma edge can be explained by the formation of internal transport barriers in this region. Such barriers come ultimately from the existence of non-monotonic profiles for both electric and magnetic fields. We used a simple theoretical description of the latter, that is, the standard non-twist map. The non-monotonicity leads to shearless curves that provide internal transport barriers for the chaotic magnetic field lines.

Another physical model in which internal transport barriers appear is the motion of particles passively advected by the $\mathbf{E} \times \mathbf{B}$ drift flow. The non-monotonic profile in this case is for the electric field due to a biased electrode inserted

into the plasma. As this barrier moves inside the plasma, the observed turbulent-driven particle flux is reduced, as observed in both TCABR and Helimak. We also investigated the behavior of the magnetic shear in internal transport barriers related to shearless curves and found that the latter persist under magnetic shear but are modified due to reconnection processes.

Acknowledgments This work was partially supported by the following Brazilian Government Agencies: CNPq, FAPESP (State of São Paulo), CAPES, and Fundação Araucária (State of Paraná).

References

1. R.D. Hazeltine, J.D. Meiss, *Plasma Confinement* (Addison Wesley, 1992)
2. W. Horton, *Turbulent Transport in Magnetized Plasmas* (World Scientific, Singapore, 2012)
3. R. Balescu, *Transport Processes in Plasmas: Classical Transport Theory* (Elsevier, Amsterdam, 1988)
4. S.J. Camargo, B.D. Scott, D. Biskamp, *Phys. Plasmas* **3**, 3912 (1996)
5. S.J. Camargo, M.K. Tippet, I.L. Caldas, *Phys. Plasmas* **7**, 2849 (2000)
6. A.J. Wootton, S.C. McCool, S. Zheng, *Fus. Technol.* **19**, 973 (1991)
7. F. Wagner, U. Stroth, *Plasma Phys. Control. Fusion.* **35**, 1321 (1993)
8. W. Horton, *Rev. Mod. Phys.* **71**, 735 (1999)
9. W. Horton, A. Hasegawa, *Chaos* **4**, 227 (1994)
10. D. Ruelle, F. Takens, *Comm. Math. Phys.* **20**, 167 (1971)
11. E.N. Lorenz, *J. Atmos. Sci.* **20**, 130 (1963)
12. A. Hasegawa, K. Mima, *Phys. Rev. Lett.* **39**, 205 (1977). *Phys. Fluids*, **21**, 81, 1978
13. K. Katou, *J. Phys. Soc. Jpn.* **51**, 996 (1982)
14. G.I. de Oliveira, F.B. Rizzato, L.P.L. de Oliveira, *Phys. D* **104**, 119 (1997)
15. R.L. Erichsen, G. Brunnet, F.B. Rizzato, *Phys. Rev. E* **60**, 6566 (1999)
16. A.M. Batista, I.L. Caldas, S.R. Lopes, R.L. Viana, W. Horton, P.J. Morrison, *Phys. Plasmas* **13**, 042510 (2006)
17. K.S. Karpylyuk, V.N. Oraevskii, V.P. Pavlenko, *Plas. Phys.* **15**, 113 (1973)
18. D. Walters, G.J. Lewak, *J. Plas. Phys.* **18**, 525 (1977)
19. A.M. Batista, I.L. Caldas, S.R. Lopes, R.L. Viana, *Phil. Trans. Royal Soc. London A* **366**, 609 (2008)
20. P.J. Morrison, *Phys. Plasmas* **7**, 2279 (2000)
21. D. del-Castillo-Negrete, *Phys. Plasmas* **7**, 1702 (2000)
22. W. Horton, H.B. Park, J.M. Kwon, D. Strozzi, P.J. Morrison, D.I. Choi, *Phys. Plasmas* **5**, 3910 (1998)
23. D. del-Castillo-Negrete, P.J. Morrison, *Phys. Fluids A* **5**, 948 (1993)
24. J.S.E. Portela, I.L. Caldas, R.L. Viana, *Eur. Phys. J. Special Topics* **165**, 195 (2008)
25. Szezech Jr. J.D., I.L. Caldas, S.R. Lopes, R.L. Viana, P.J. Morrison, *Chaos* **19**, 043108 (2009)
26. J. D. Szezech Jr., I.L. Caldas, S.R. Lopes, P.J. Morrison, R.L. Viana, *Phys. Rev. E* **86**, 036206 (2012)
27. W. Horton, *Plas. Phys. Contr. Fusion* **27**, 937 (1985)

28. A. Marcus, I.L. Caldas, Z. Guimarães-Filho, P.J. Morrison, W. Horton, Yu. Kuznetsov, I.C. Nascimento, *Phys. Plasmas* **15**, 112304 (2008)
29. I.C. Nascimento, I.L. Caldas, R.M.O. Galvão, *J. Fusion Energy* **12**, 529 (1993)
30. R.L. Viana, S.R. Lopes, I.L. Caldas, Szezech Jr. J.D., Z. Guimarães-Filho, G.Z. dos Santos Lima, P.P. Galuzio, A.M. Batista, Yu. Kuznetsov, I.C. Nascimento, *Comm. Nonlin. Sci. Num. Simul.* **17**, 4690 (2012)
31. Z.O. Guimarães-Filho, I.L. Caldas, R.L. Viana, M.V.A.P. Heller, I.C. Nascimento, Yu.T. Kuznetsov, R. Bengtson, *Phys. Plasmas* **15**, 062501 (2008)
32. F.A. Marcus, T. Kroetz, M. Roberto, I.L. Caldas, E.C. da Silva, R.L. Viana, Z.O. Guimaraes-Filho, *Nucl. Fusion* **48**, 024018 (2008)
33. I.L. Caldas, R.L. Viana, C.V. Abud, J.C.D. Fonseca, Z.O. Guimarães-Filho, T. Kroetz, F.A. Marcus, A. Schelin, J.D. Szezech Jr., D.L. Toufen, M.S. Benkadda, S.R. Lopes, P.J. Morrison, M. Roberto, K. Gentle, Yu. Kuznetsov, I.C. Nascimento, *Plas. Phys. Contr. Fusion* **54**, 124035 (2012)
34. K.W. Gentle, K. Liao, K. Lee, W.L. Rowan, *Plasma Sci. Technol.* **12**, 391 (2010)
35. K.W. Gentle, H. He, *Plasma Sci. Technol.* **10**, 284 (2008)
36. Ch.P. Ritz, E.J. Power, T.L. Rhodes, R.D. Bengtson, K.W. Gentle, H. Li, P.E. Phillips, A.J. Wootton, D.L. Brower, N.C. Luhmann Jr., W.A. Peebles, P.M. Schoch, R.L. Hickok, *Rev. Sci. Instrum.* **59**, 1739 (1988)
37. D.L. Toufen, Z.O. Guimarães-Filho, I.L. Caldas, J.D. Szezech, S.R. Lopes, R.L. Viana, K.W. Gentle, *Phys. Plasmas* **20**, 022310 (2013)